arXiv:2105.03472v2 [cond-mat.supr-con] 19 Aug 2021

Electronic structure, electron-phonon coupling and superconductivity in noncentrosymmetric $ThCoC_2$ from *ab initio* calculations

Gabriel Kuderowicz, Paweł Wójcik, and Bartlomiej Wiendlocha*
Faculty of Physics and Applied Computer Science,
AGH University of Science and Technology, Aleja Mickiewicza 30, 30-059 Krakow, Poland
(Dated: February 2, 2022)

Superconductors without inversion symmetry in their crystal structure are known to exhibit unconventional properties. Recently, based on the measured temperature dependence of the magnetic field penetration depth, superconductivity in noncentrosymmetric $ThCoC_2$ was proposed to be a nodal *d*-wave and mediated by the spin fluctuations. Moreover, a non-BCS behavior of the temperature dependence of the electronic specific heat and the magnetic upper critical field were reported. In this work, the electronic structure, phonons and electron-phonon coupling are studied in $ThCoC_2$ on the basis of *ab initio* computations. The effect of the spin-orbit coupling on the electronic structure and electron-phonon interaction is analyzed, and a large splitting of the electronic band structure is found. The calculated electron-phonon coupling constant $\lambda = 0.59$ remains in decent agreement with the experimental estimates, suggesting that the electron-phonon interaction is strong enough to explain superconductivity with $T_c \simeq 2.5$ K. Nevertheless, we show that the conventional isotropic Eliashberg formalism is unable to describe the thermodynamic properties of the superconducting state, as calculated temperature dependence of the electronic specific heat and magnetic penetration depth deviate from experiments, which is likely driven by the strong spin-orbit coupling and inversion symmetry breaking. In addition, to shed more light on the pairing mechanism, we propose to measure the carbon isotope effect, as our calculations based on the electron-phonon coupling predict the observation of the isotope effect with an exponent $\alpha \simeq 0.15$.

I. INTRODUCTION

In recent years, noncentrosymmetric superconductors (NCSs) have attracted a growing interest as host materials for studying the interplay between the spin-orbit coupling (SOC) and the superconducting state of matter. The lack of inversion symmetry in NCSs together with the corresponding antisymmetric spin-orbit coupling (ASOC) removes the parity constraint on the Cooper pair and allows for a mixture of spin-singlet and spin-triplet states [1–5]. This unusual Cooper pair formation results in an unconventional superconductivity which may manifest itself by the gap with nodal lines or points, multiband effects, or the extraordinary high magnetic critical field. Among NCSs discovered up-to-date, a special place is given for the heavy fermion superconductors with the first discovered $CePt_3Si$ [6] as well as $CeRhSi_3$ [7] or $CeCoGe_3$ [8]. The superconducting state in these compounds coexists with the magnetic ordering and is generated by the strong electronic correlations which make the physical effects coming from the solely noncentrosymmetric structure difficult to extract. To overcome this obstacle, most recent studies are directed towards weakly correlated NCSs, including $Li_2(Pd,Pt)_3B$ [9–13], $Mg_{10}Ir_{19}B_{16}$ [14], $La(Ir,Rh)(P,As)$ [15], Ru_7B_3 [16, 17], Y_2C_3 [18, 19], Mo_3Al_2C [20], $(Nb,Ta)Rh_2B_2$ [21], $(Nb,Ta)Ir_2B_2$ [22], or $LaNiC_2$ [23–32], which is isostructural and isoelectronic with $ThCoC_2$.

Although $LaNiC_2$ belongs to a group of superconductors with relatively weak electron-phonon coupling ($T_c = 2.8$ K, $\lambda \simeq 0.50$), it exhibits non-BCS superconducting properties, reported independently in the specific heat [23] and penetration depth measurements [26–28]. Despite this, up to now there is no general agreement whether the unconventional phase in $LaNiC_2$ is caused by the multiband Fermi surface, spin-triplet pairing or time-reversal symmetry breaking [31, 32]. The most recent muon spin rotation (μSR) measurements on single crystals of $LaNiC_2$ point to the two nodeless gaps with the broken time-reversal symmetry [34]. Another striking behavior of $LaNiC_2$ has been discovered under the external pressure, which initially increases the critical temperature to suppress superconductivity above 7 GPa [29]. The evolution of T_c with pressure and the thermodynamic properties of $LaNiC_2$, with the special attention

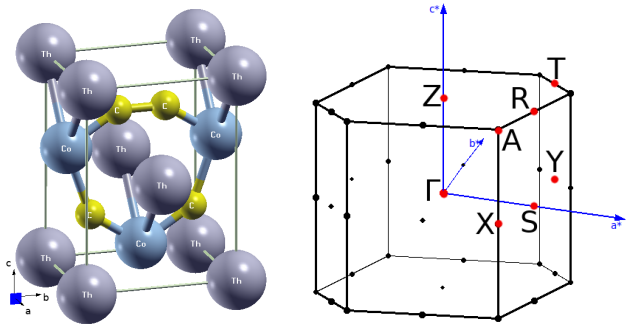


FIG. 1. The unit cell of $ThCoC_2$ visualized with XCrysDen [33] and the Brilloiun zone (BZ) with high symmetry points.

* wiendlocha@fis.agh.edu.pl

paid to their non-BCS character, have been analyzed in Ref. [30], on the basis of the *ab initio* calculations and the isotropic Eliashberg formalism. It was found that the measured non-BCS temperature dependence of the London magnetic penetration depth [28] is close to that predicted by the Eliashberg theory, which made it more difficult to clearly classify $LaNiC_2$ as an unconventional superconductor.

Recent years directed studies on NCSs towards the $ThCoC_2$ compound, which crystallizes in the same base centered orthorhombic structure (*Amm2*, spacegroup no. 38), as $LaNiC_2$. Unit cell is shown in Fig. 1. They both belong to a large series of rare-earth carbides $RCoC_2$ and $RNiC_2$, recently intensively studied mainly due to their interesting magnetic properties [35–39]. $ThCoC_2$ is a nonmagnetic, type-II superconductor with a critical temperature $T_c \simeq 2.5$ K (reported T_c slightly varies between the samples, being 2.65 K in Ref. [40], 2.55 K in Ref. [41] and 2.3 K in Ref. [42]). It shows several non-BCS thermodynamic properties in the superconducting state. The upper magnetic critical field (H_{c2}) measured as a function of temperature exhibits a positive curvature [40] which is commonly attributed to the interband coupling occurring in multiband systems, similar to MgB_2 [28, 43, 44]. The electronic specific heat measurement reveals a strong non-BCS behavior with the normalized specific heat jump $\Delta C_e/\gamma T_c = 0.86$ and a significant deviation from the exponential trend of $C_e(T)$ at low temperatures [40]. Importantly, the normalized residual Sommerfeld coefficient γ_0 exhibits a square root magnetic field dependence $\gamma_0 \sim \sqrt{H}$ [41], which is commonly considered a hallmark of nodes in the superconducting order parameter. The nodal line scenario has been recently strengthen by the μSR measurement where the temperature dependence of the magnetic penetration depth was well fitted assuming a $d-$wave superconducting gap symmetry [42]. Moreover, spin-fluctuation mechanism of electron paring was proposed in that work.

The aim of the present paper is to theoretically investigate the electronic structure, lattice dynamics, electron-phonon interaction and superconductivity in $ThCoC_2$, assuming that superconductivity is mediated by the electron-phonon interaction. In the first step, *ab-initio* calculations of the electronic band structure and the electron-phonon coupling were performed, and the spin-orbit coupling effects were analyzed. Next, the thermodynamic parameters of the superconducting state were determined using the isotropic Eliashberg formalism where all depairing effects were approximated by the Coulomb pseudopotential μ^*. We find that already within the Eliashberg framework the superconducting state in $ThCoC_2$ exhibits non-BCS characteristics. However, in contrast to $LaNiC_2$, experimental results strongly deviate both form the BCS predictions and isotropic Eliashberg solutions, showing the importance of the inversion symmetry breaking accompanied by the strong spin-orbit coupling, effects not taken into account in both theories.

The paper is organized as follows. In Sec.II we provide basic information about $ThCoC_2$ structure and give all the computational details used in the paper. Electronic structure of the considered compound is described in Sec. III while phonons and electron-phonon coupling are analyzed in Sec. IV. Section V contains the analysis of thermodynamic parameters calculated within the Eliashberg formalism, discussing recent experiments in the latter case. The summary is included in Sec. VI.

II. COMPUTATIONAL DETAILS

Calculations in this work were done using the Density Functional Theory (DFT) and Quantum Espresso package [45, 46]. We used Perdew-Burke-Ernzerhof (PBE) generalized gradient approximation for the exchange-correlation functional [47] and Rappe-Rabe-Kaxiras-Joannopoulos (RRKJ) ultrasoft pseudopotentials [48, 49]. Calculations were done both in the scalar-relativistic and fully-relativistic approach (that is, with the spin-orbit coupling included). In the latter case, relativistic pseudopotentials for Th and Co were used.

First, unit cell parameters and atomic positions were optimized within Broyden-Fletcher-Goldfarb-Shanno algorithm, starting from the experimental values [50]. Since in the available literature the atomic positions in $ThCoC_2$ are not reported, those of $LaNiC_2$ were taken as the initial ones. Optimized cell parameters are close to the experimental ones and are given in Table I. Atomic positions were additionally relaxed with SOC, but no changes were observed.

For the relaxed unit cell, the electronic structure was calculated using a Monkhorst-Pack grid of 12^3 k-points, whereas the Fermi surface was calculated on a denser 18^3 mesh. Plane-wave expansion energy and charge density cutoffs were set to 130 Ry and 1300 Ry, respectively. Such large values were required due to the presence of the Th atom. Interatomic force constants (IFC) were computed using the density functional perturbation theory [51] from the Fourier interpolation of 21 inequivalent dynamical matrices, which make up a 4^3 q-point grid. Phonon dispersion relations were calculated from IFC by Fourier interpolation. Finally, the Eliashberg electron-phonon interaction function $\alpha^2F(\omega)$ was determined using the self-consistent first order variation of the crystal potential from the preceding phonon calculations. The spectral function $\alpha^2F(\omega)$ was then used to determine the electron-phonon coupling (EPC) parameter λ and

TABLE I. Experimental and calculated unit cell parameters. Atomic positions (in crystal coordinates) are in a form: Th (0,0,u), Co (0.5,0,v), C (0.5,±y,z).

	a (Å)	b (Å)	c (Å)	u	v	y	z
expt.	3.8063	4.5329	6.1461	0.0	0.626	0.160	0.289
calc.	3.8214	4.5376	6.0708	-0.0014	0.6041	0.1561	0.3007

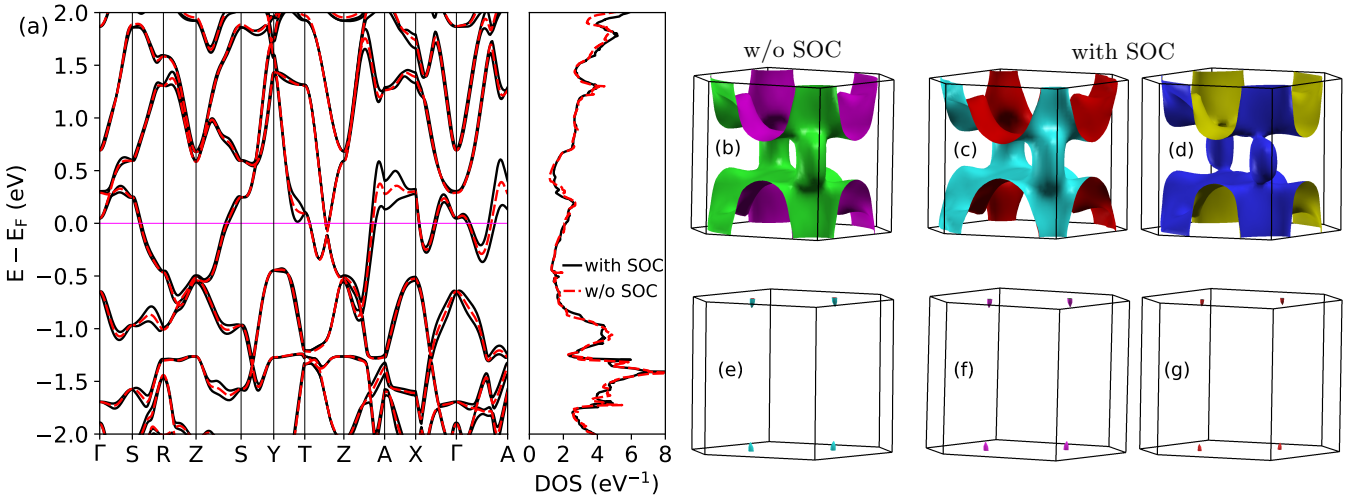


FIG. 2. (a) Electronic dispersion relation and density of states of $ThCoC_2$ calculated with and without SOC. Magenta line marks the Fermi energy. Panels (b) and (e) show Fermi surface sheets without SOC, whereas (c), (d), (f) and (g) present the splitting of the Fermi surface caused by SOC.

thermodynamic parameters of the superconducting phase based on the Eliashberg formalism.

III. ELECTRONIC STRUCTURE

Figure 2(a) shows the electronic band structure and density of states (DOS) of $ThCoC_2$ calculated with and without SOC. Brillouin zone of the system, with the location of high-symmetry points, is presented in Fig. 1(b). As shown, in the scalar-relativistic case, two bands cross the Fermi level, forming the Fermi surface (FS) that consists of a complex hole-like sheet [Fig.2(b)] and two very small electron pockets localized on T-Z path in the Brillouin zone [Fig.2(e)]. Interestingly, the hole-like sheet reveals a quasi-two-dimensional topology in the form of two parts connected by tubes, all aligned along the $\boldsymbol{k}_z$ axis, what suggests anisotropy in the transport properties. Note that our Fermi surface is similar to the one reported by Bhattacharyya et al. [42] even though they employed LDA+U method, which resulted e.g. in removing the small electron pockets from the FS.

In the relativistic case, the presence of the antisymmetric SOC leads to the splitting of electronic bands. The two bands crossing the Fermi level split into four which results in four spin-split Fermi surface sheets, plotted in Fig. 2(c,d,f,g). Except for the band splitting, SOC does not change the shape of the Fermi surface much, which looks very similar to that calculated for $LaNiC_2$ [30]. However, the magnitude of SOC splitting energy ΔE_{SOC} is considerably larger. ΔE_{SOC} for the band which forms the dominating FS sheet [Fig. 2(b-d)], plotted along the same path as used in Fig. 2(a) is shown in Fig. 4(a) and reaches its maximal value of 450 meV near the A point in BZ.

To calculate the average value of SOC splitting, we have computed the energy eigenvalues on a regular grid of about 7000 $k-$points, sampling the primitive cell in the reciprocal space. To get the representative value around the Fermi level only, we have imposed a condition that one of the energy eigenvalues has to be below and the other above E_F. About 700 points have met that condition, and the average splitting, computed from the energy differences between the pair of states, as well as the median, is about 150 meV. The distribution of ΔE_{SOC} in the Brillouin zone is marked on the scalar-relativistic Fermi surface in Fig. 4(b). Computed $\overline{\Delta E_{\mathrm{SOC}}}$ is considerably larger than in $LaNiC_2$, where the average was about 40 meV [30, 52], and closer to that in triplet superconductors $CePt_3Si$ and Li_2Pt_3B (200 meV). The combination of a large ΔE_{SOC} and a relatively low T_c results in a large value of the characteristic E_r ratio [53] $E_r = \overline{\Delta E_{\mathrm{SOC}}}/k_B T_c \simeq 700$. The large value of E_r was observed to be correlated with the presence of a triplet component in several NCSs [53]. E_r is equal to 177 in

TABLE II. Total and projected densities of states at the Fermi energy of $ThCoC_2$, Sommerfeld coefficient γ ("bare" band-structure values) calculated with and without SOC, and the electron phonon coupling constant λ, computed as a renormalization factor from the experimental $\gamma_{\mathrm{expt}} = \gamma_{\mathrm{band}}(1+\lambda)$. Third row shows the experimental values of γ and λ, the latter is extracted from the experimental T_c and McMillan formula (see text).

	$N(E_F)$ (eV^{-1})				γ	λ
	Total	Th	Co	C_2	$\left(\frac{\mathrm{mJ}}{\mathrm{mol\,K^2}}\right)$	
w/o SOC	2.07	0.86	0.74	0.43	4.88	0.72
with SOC	2.14	0.89	0.77	0.45	5.04	0.66
expt. [41]		-			8.38	0.49

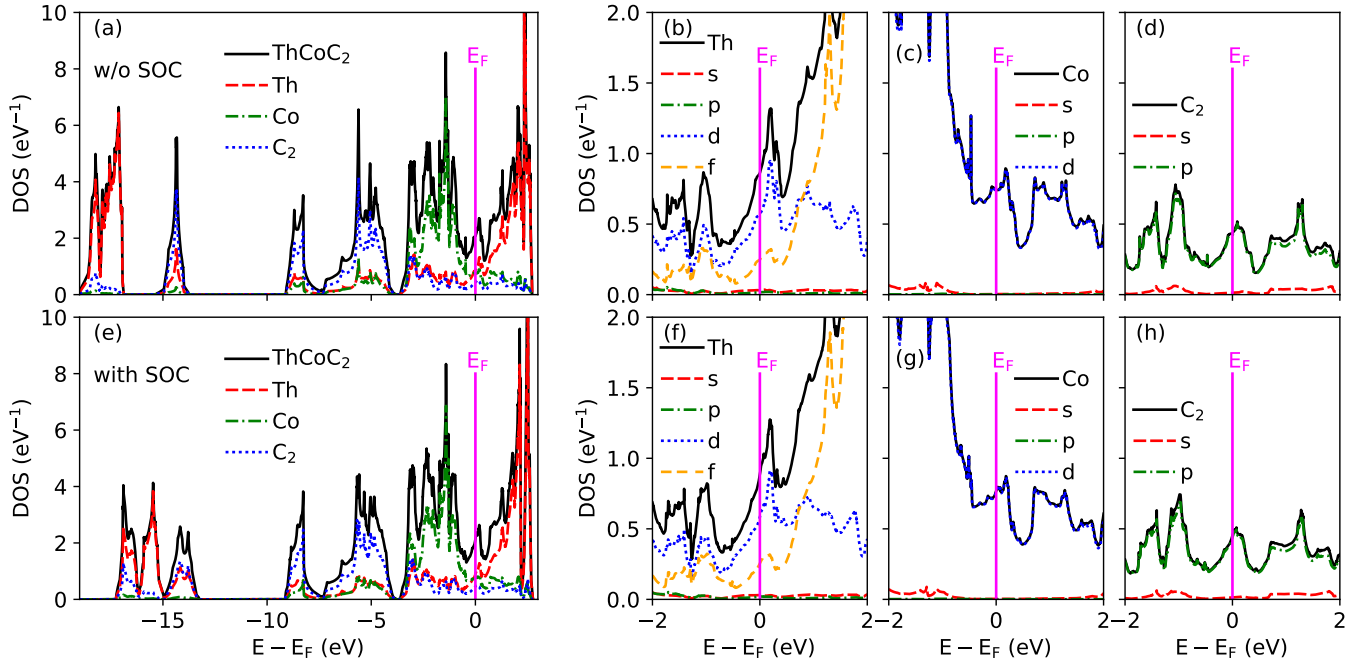


FIG. 3. Total and projected density of states of $ThCoC_2$: (a)-(d) without SOC and (e)-(h) with SOC.

$LaNiC_2$, ~ 890 in Li_2Pt_3B and ~ 3000 in $CePt_3Si$.

Density of states plotted in Fig. 3 indicates that the largest contribution to the total DOS at the Fermi level, $N(E_F) = 2.1$ eV^{-1}, comes from $6d$ Th, $3d$ Co and $2p$ C states. Due to the charge transfer from the $7s$ shell, $5f$ states of Th are partially filled and contribute to $N(E_F)$ in about 12%. The Th-$5f$ shell filling is equal about 0.8, similar to that found in elemental Th [55] or recently studied $ThIr_3$ superconductor [56]. Those $5f$ states have an itinerant character, thus no strong electronic correlations associated with the f-shell are expected, in agreement with the measured rather low value of the Sommerfeld coefficient (see below). Along with the small effect on the shape of Fermi surface, SOC changes $N(E_F)$ only slightly (see Table II). The obtained $N(E_F)$ is relatively low and lower than e.g. in $LaNiC_2$ (2.37 eV^{-1} [30]). Resulting band-structure value of the Sommerfeld coefficient $\gamma_{\rm band} = \frac{\pi^2}{3} k_B^2 N(E_F)$ is $\gamma_{\rm band} = 5.04$ mJ mol^{-1} K^{-2}, whereas the experimental one [40] is $\gamma_{\rm expt} = 8.38$ mJ mol^{-1} K^{-2}. Under the assumption that the electronic specific heat is renormalized only by the electron-phonon interaction, $\gamma_{\rm expt} = \gamma_{\rm band}(1+\lambda)$, we obtain the estimation of the electron-phonon coupling parameter $\lambda = 0.66$, which is in the moderate-coupling regime. Table II also presents the "experimental" value [41] of $\lambda = 0.49$, which was recalculated from the McMillan's formula for T_c using the experimental value of T_c, Debye temperature of $\theta_D = 449$ K and the Coulomb pseudopotential parameter $\mu^* = 0.13$.

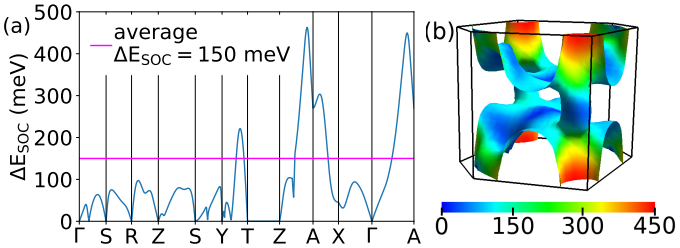


FIG. 4. $\Delta E_{\rm SOC}$: SOC-induced splitting of the energy band, which gives the dominating contribution to $N(E_F)$: (a) along the high-symmetry directions regardless of the actual energy value; (b) computed under the condition that the two spin-split bands are on the opposite side of the Fermi energy, and marked on the scalar-relativistic Fermi surface, plotted using FermiSurfer [54]. The average value of $\overline{\Delta E_{\rm SOC}} = 150$ meV is calculated based on results visualized in panel (b).

IV. PHONONS AND ELECTRON-PHONON COUPLING

Figure 5 presents the phonon dispersion curves $\omega(\mathbf{q})$ and the phonon density of states $F(\omega)$ calculated with SOC, although influence of the spin-orbit interaction occurred to be negligible for the phonon structure. The obtained phonon spectrum is stable with no imaginary frequencies. As there are four atoms in the primitive cell, 12 phonon branches are displayed in Fig. 5, shaded with respect to the atomic character. The corresponding partial atomic $F(\omega)$ is also presented in the right panel.

Due to the large differences in the atomic masses between Th (232 u), Co (58.9 u), and C (12 u), the phonon spectrum is separated into three parts. The six high-

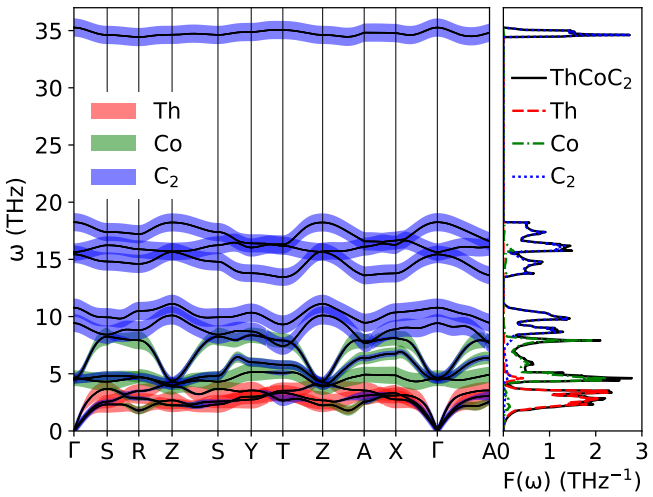


FIG. 5. Phonon dispersion relations with colored atomic contributions (left panel) and the corresponding phonon density of states (right panel). Results for $ThCoC_2$ with SOC.

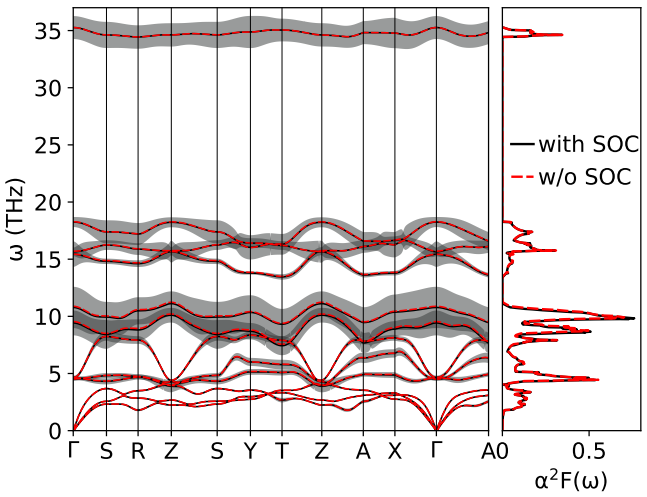


FIG. 6. Electron-phonon coupling in $ThCoC_2$. Left panel: phonon dispersion relations with the phonon linewidths $\gamma_{\boldsymbol{q}\nu}$ marked by shading. Phonon linewidths are multiplied by 20. Right panel: Eliashberg function computed with and without SOC.

est frequency phonon branches are dominated by carbon atoms' vibrations, with the single mode near 35 THz attributed to the bond-stretching C-C oscillations, just like observed in $LaNiC_2$ [30]. Cobalt dominates among the modes located between 5 and 10 THz, whereas the lowest part of the spectrum is mostly contributed by thorium. The average phonon frequencies are shown in Table III and one can see that SOC only slightly lowers the average values.

Electron-phonon interaction is described within the isotropic Eliashberg function, defined as

$$\alpha^2F(\omega) = \frac{1}{2\pi N(E_F)} \sum_{\boldsymbol{q}\nu} \delta(\omega - \omega_{\boldsymbol{q}\nu}) \frac{\gamma_{\boldsymbol{q}\nu}}{\hbar\omega_{\boldsymbol{q}\nu}}, \qquad (1)$$

where $\omega_{\boldsymbol{q}\nu}$ is the phonon frequency for the mode ν at the wave vector $\boldsymbol{q}$ while $\gamma_{\boldsymbol{q}\nu}$ is the phonon linewidth which describes the strength of the interaction between the electrons from the Fermi surface and a phonon mode ν at $\boldsymbol{q}$:

$$\gamma_{\boldsymbol{q}\nu} = 2\pi\omega_{\boldsymbol{q}\nu} \sum_{ij} \int \frac{d^3k}{\Omega_{BZ}} |g_{\boldsymbol{q}\nu}(\boldsymbol{k}, i, j)|^2 \times \delta(E_{\boldsymbol{q},i} - E_F)\delta(E_{\boldsymbol{k}+\boldsymbol{q},j} - E_F). \qquad (2)$$

In the above expression, $g_{\boldsymbol{q}\nu}(\boldsymbol{k}, i, j)$ are the interaction matrix elements given by [57]

$$g_{\boldsymbol{q}\nu}(\boldsymbol{k}, i, j) = \sum_s \left(\frac{\hbar}{2M_s\omega_{\mathbf{q}\nu}}\right)^{1/2} \langle\psi_{i,\mathbf{k}}| \frac{dV_{scf}}{d\hat{u}_{\nu,s}} \cdot \hat{\epsilon}_\nu |\psi_{j,\mathbf{k}+\mathbf{q}}\rangle, \qquad (3)$$

where M_s is a mass of the atom s, $\psi_{i,\mathbf{k}}$ is an electron wave function at $\mathbf{k}$-point, $\hat{\epsilon}_\nu$ is a polarization vector of a phonon mode and $\frac{dV_{scf}}{d\hat{u}_{\nu,s}}$ is a change of the electronic potential, calculated in the self-consistent manner, due to the displacement of the atom s in the $\hat{u}_{\nu,s}$ direction. While the Eliashberg function expresses the electron-phonon coupling summed over Brillouin zone and phonon modes ν, the electron-phonon coupling constant (EPC) λ is a single parameter characterizing the overall coupling strength, and is given by

$$\lambda = 2\int_0^{\omega_{max}} \frac{\alpha^2F(\omega)}{\omega} d\omega. \qquad (4)$$

Figure 6 displays the phonon dispersion curves with shading corresponding to the phonon linewidths, $\gamma_{\boldsymbol{q}\nu}$, together with the Eliashberg spectral function presented in the right panel. As we mentioned above, SOC had almost no effect on the phonon dispersion curves, the same holds for the magnitude of the electron-phonon coupling, with no visible differences for the scalar-relativistic and relativistic $\alpha^2F(\omega)$. All these are a consequence of the fact that lighter atoms' (Co and C) electronic states give the largest contribution to the Fermi surface, and the contribution from Th is not a dominant one. Much different situation was found in e.g. $CaBi_2$ [58] or $LaBi_3$ [59], where due to domination of Bi-6p orbitals the electron-phonon coupling constant was modified by SOC in almost 50%. The computed linewidths $\gamma_{\boldsymbol{q}\nu}$ show that the electron-phonon coupling is relatively the strongest

TABLE III. Average phonon frequencies.

	Total (THz)	Th (THz)	Co (THz)	C (THz)
with SOC	10.59	3.00	6.41	16.55
w/o SOC	10.62	3.00	6.42	16.60

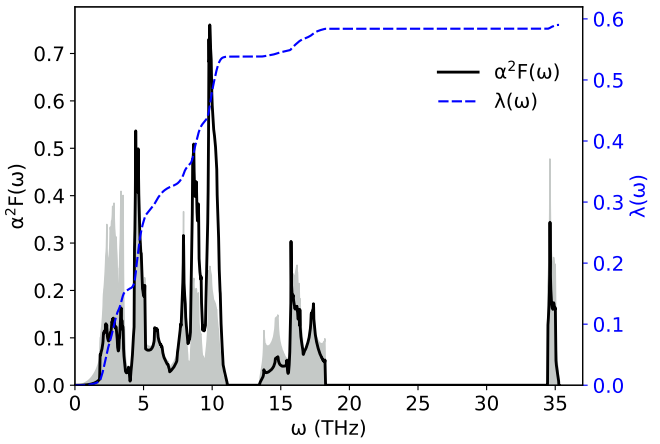


FIG. 7. Eliashberg function of $ThCoC_2$ and cumulative electron-phonon coupling constant. Shading displays phonon density of states normalized to the integral of the Eliashberg function. Results for the case with SOC.

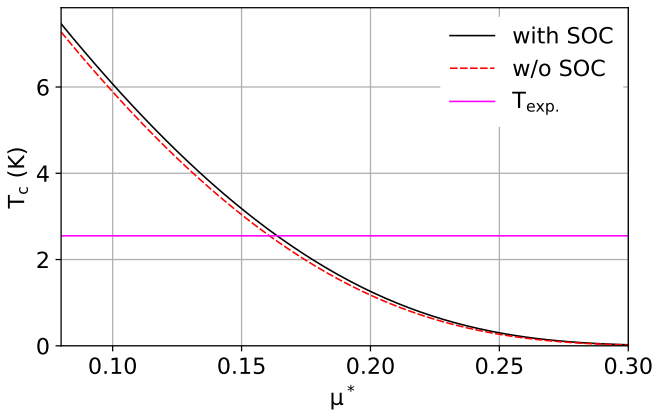


FIG. 8. Critical temperature of $ThCoC_2$ calculated as a function of the μ^* parameter from the Allen-Dynes formula. Magenta line marks the experimental value $T_c = 2.55$ K.

for the carbon atoms' modes, located around 10 THz. The highest C mode, located near 35 Hz, despite having large $\gamma_{\boldsymbol{q}\nu}$, does not give a significant contribution to the electron-phonon coupling as $\alpha^2F(\omega)$ is inversely proportional to ω, and $\lambda \propto \frac{\gamma_{\boldsymbol{q}\nu}}{\omega^2_{\boldsymbol{q}\nu}}$, see Eq.(1-4). Additionally, in Fig. 7 Eliashberg function is plotted with the phonon DOS in the background and the cumulative electron-phonon coupling parameter $\lambda(\omega)$. Here one can clearly see the relative enhancement of $\alpha^2F(\omega)$ above the bare $F(\omega)$ near 10 THz due to the large $\gamma_{\boldsymbol{q}\nu}$ of carbon. As presented in Fig. 6 and Fig. 7, the meaningful contribution to the electron-phonon coupling comes also from the Co vibrations. Although Co modes couple to electrons to a smaller extent, having a significantly narrower linewidth, the lower frequencies in its phonon branches partly compensate smaller $\gamma_{\boldsymbol{q}\nu}$ giving raise to a large peak in $\alpha^2F(\omega)$ near 5 THz. Relatively, the weakest coupling is seen for Th modes, for which Eliashberg function goes visibly below $F(\omega)$ in Fig. 7, nevertheless due to their lowest phonon frequencies thorium modes do contribute to the total λ. As one can see from the cumulative $\lambda(\omega)$ plot, the electron phonon coupling constant is determined mostly by the phonon modes from 0 to 10 THz with important contributions from Th, Co and the two lowest C modes. The calculated total EPC parameter is $\lambda = 0.59$ and is only slightly enhanced by SOC, see Table IV. This value is close to $\lambda = 0.49$, determined from T_c using the inverted McMillan formula in Ref. [41], and is slightly lower than extracted above as a renormalization factor of the Sommerfeld coefficient, $\lambda = 0.66$. All these values suggest that $ThCoC_2$ is in the intermediate electron-phonon coupling regime. In Table IV we also include the computed values of the renormalized Sommerfeld coefficient $\gamma = \gamma_{\text{band}}(1 + \lambda)$, where γ_{band} were determined from the computed DOS in Table II, and λ from the Eliashberg function. The theoretical value of 8.0 (mJ mol^{-1} K^{-2}) is slightly lower than the experimental one, which is 8.4 (mJ mol^{-1} K^{-2}).

Next, we may calculate the superconducting critical temperature which would correspond to the calculated λ under the assumption of the conventional s-wave superconducting gap symmetry. Although for the noncentrosymmetric compounds the Allen-Dynes formula is used beyond its applicability, it is commonly applied to estimate T_c while the value of μ^* parameter provides an additional information about the degree of deviation of superconductivity from the conventional one as well as about the strength of electronic interactions. The Allen-Dynes formula [60] has the following form

$$k_B T_c = \frac{\hbar\langle\omega_{\log}^{\alpha^2F}\rangle}{1.20} \exp\left\{-\frac{1.04(1+\lambda)}{\lambda - \mu^*(1+0.62\lambda)}\right\}, \qquad (5)$$

where μ^* is the Coulomb pseudopotential parameter and $\langle\omega_{\log}^{\alpha^2F}\rangle$ is the logarithmic average

$$\langle\omega_{\log}^{\alpha^2F}\rangle = \exp\left(\frac{2}{\lambda}\int_0^{\omega_{max}} \alpha^2F(\omega)\ln\omega\frac{d\omega}{\omega}\right). \qquad (6)$$

T_c as a function of the Coulomb pseudopotential μ^* is plotted in Fig. 8. For the typically used values of μ^* (0.10 recommended for use with the Allen-Dynes formula [60] or 0.13 commonly-used with the McMillan equation) T_c is overestimated roughly two times. There are several possible explanations for this overestimating tendency. The first is that the electron-phonon coupling is weaker in the real material than the calculated λ. However, as the computed renormalized Sommerfeld parameter is lower than the experimental one (8.0 *versus* 8.4 mJ mol^{-1} K^{-2}), this is not expected. The second is that the Coulomb pseudopotential μ^* is enhanced. The experimental value of $T_c = 2.5$ K is reproduced for $\mu^* = 0.165$, a value larger than typically observed in intermetallic superconductors. As frequently considered in such cases, this may originate from the presence of other depairing mechanisms which for the considered compound can

TABLE IV. Logarithmic average $\langle\omega_{\log}^{\alpha^2F}\rangle$, electron-phonon coupling constant λ, superconducting critical temperature T_c from eq. (5) with $\mu^* = 0.13$, and Sommerfeld coefficient γ renormalized with λ from the electron-phonon calculations, $\gamma = \gamma_{\rm band}(1+\lambda)$. Experimental values repeated for convenience.

	$\langle\omega_{\log}^{\alpha^2F}\rangle$ (THz)	λ	T_c (K)	γ $\left(\frac{\rm mJ}{\rm mol\,K^2}\right)$
w/o SOC	5.849	0.583	4.05	7.73
with SOC	5.816	0.590	4.23	8.01
expt. [41]	-	0.493	2.55	8.38

be the electron-paramagnon interactions (spin fluctuations) [56, 61–66], recently suggested as the pairing mechanism for $ThCoC_2$ [42]. Assuming spin fluctuations as an additional renormalization factor for the electronic specific heat, $\gamma_{\rm expt} = \gamma_{\rm band}(1+\lambda+\lambda_{\rm sf})$, a small value of $\lambda_{\rm sf} = 0.07$ is obtained. This hypothesis, however, requires further experimental analysis by measurements of the electrical resistivity and magnetic susceptibility. It is worth recalling that for Nb and its alloys values of μ^* as large as ~ 0.20 has to be used to reproduce the experimental T_c [67, 68]. Finally, the last and the most probable reason for the need of applying enhanced μ^* is the inapplicability of the Allen-Dynes formula for the $ThCoC_2$ case. The strong spin-orbit interaction, leading to the average band splitting of 150 meV, is comparable to the maximal phonon energy (35 THz $\simeq$ 145 meV) and larger than the average phonon energy of 44 meV, with $\overline{\Delta E_{\rm SOC}}/k_BT_c \simeq 700$. Thus, it will effectively compete with the formation of the conventional superconducting phase, as in the limit of the strong spin-orbit interaction [2] the pairing inside the spin-split bands requires the odd parity with respect to the $\mathbf{k} \to -\mathbf{k}$. As a consequence, the Allen-Dynes formula, derived for a conventional case, may overestimate T_c, which was not the case for $LaNiC_2$, where experimental T_c was obtained for $\mu^* = 0.13$ [30, 69]. However, the electron-phonon interaction seems to be strong enough to be responsible for superconductivity in $ThCoC_2$ with the observed T_c, supporting the idea of the conventional pairing mechanism, but the analysis of the thermodynamic properties of the superconducting state, presented in the next Section, reveals further deviations from the simplest isotropic s-wave picture.

V. ELIASHBERG FORMALISM

In this section, we determine thermodynamic parameters of $ThCoC_2$ in the superconducting state within the isotropic Eliashberg formalism [70], and compare our results with the latest experiments. The usage of the Eliashberg equations is considered as a first approximation towards the understanding of superconductivity in $ThCoC_2$, since similarly to the Allen-Dynes formula, they are not fully applicable for the case of a noncentrosymmetric compound with strong SOC. However, comparing the results obtained using this approach with the experiment allows to directly show how strong are the deviations of superconducting properties of $ThCoC_2$ from the conventional isotropic ones.

A. Eliashberg equations

Our calculations are based on the isotropic Eliashberg equations which, on the imaginary axis ($i = \sqrt{-1}$), are given by

$$Z(i\omega_n) = 1 + \frac{\pi k_B T}{\omega_n}\sum_{n'}\frac{\omega_{n'}}{R(i\omega_{n'})}\lambda(n-n') \quad (7)$$

$$Z(i\omega_n)\Delta(i\omega_n) = \pi k_B T\sum_{n'}\frac{\Delta(i\omega_{n'})}{R(i\omega_{n'})}\times [\lambda(n-n') - \mu^*\theta(\omega_c - \omega_{n'})], \quad (8)$$

where $Z(i\omega_n)$ is the mass renormalization function, $\Delta(i\omega_n)$ is the superconducting order parameter, $i\omega_n = i(2n+1)\pi k_B T$ are fermionic Matsubara frequencies where $n \in \mathbb{Z}$, $\theta(\omega)$ is the Heviside function, k_B is the Boltzmann constant, T is temperature and $R(i\omega_n) = \sqrt{\omega_n^2 + \Delta^2(i\omega_n)}$.

The kernel of the electron-phonon interaction is assumed in the common form

$$\lambda(n-n') = \int_0^\infty d\omega \frac{2\omega\alpha^2F(\omega)}{(\omega_n - \omega_{n'})^2 + \omega^2}, \quad (9)$$

where $\alpha^2F(\omega)$ is the isotropic Eliashberg spectral function discussed in Sec. IV.

In Eq. (8), μ^* is the Coulomb pseudopotential which is originally defined as a double Fermi surface average of the matrix elements of the screened Coulomb interactions between electrons taking part in the scattering events $\mathbf{k} \to \mathbf{k}'$ induced by the electron-electron interaction. μ^* usually yields the value in the range $[0.1, 0.2]$ [71]. Note however that in some electron-phonon mediated superconductors, $\mu^* > 0.2$, which cannot result solely from the Coulomb interaction. Then, as commonly assumed, μ^* contains all physical effects competitive to superconductivity and not included in the Eliashberg equations. Although calculations of μ^* from the *ab-initio* methods are possible, it requires more sophisticated numerical methods [72–74] which are beyond the scope of the present paper. Instead of that, we use the common practice in which μ^* is determined based on the experimental value of T_c to be able to discuss the thermodynamic properties of the material as a function of T/T_c. Since it corresponds to the Coulomb pseudopotential in the Allen-Dynes formula, they are denoted by the same symbol, although usually different values are required to get the same T_c in both approaches [30, 75, 76], and a scaling procedure should be applied [60] to compare both values.

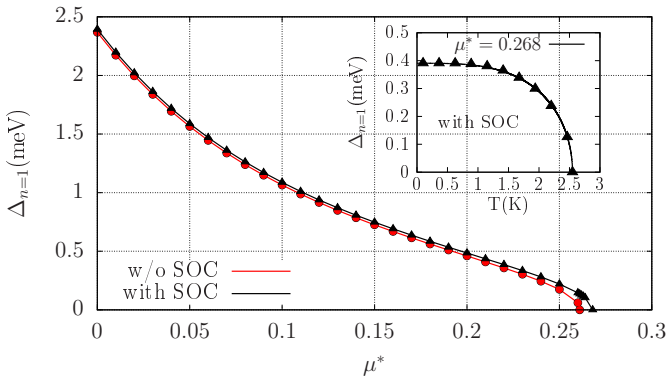


FIG. 9. The superconducting energy gap $\Delta_{n=1}$ evaluated at $T = 2.55$ K, as a function of μ^*. Results with and without SOC. Inset presents $\Delta_{n=1}(T)$ for $\mu^* = 0.268$ for which $T_c = 2.55$ K.

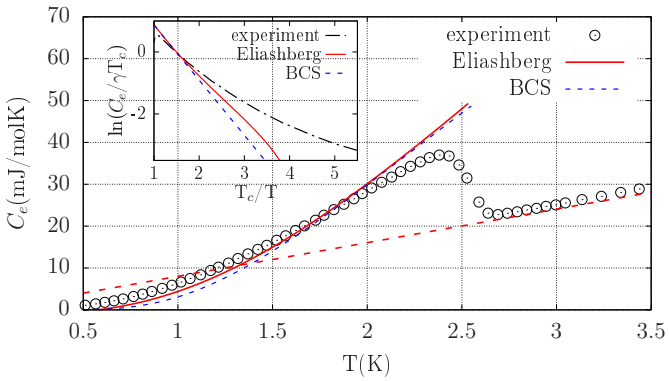


FIG. 10. Electronic specific heat C_e as a function of temperature T. The normal state is marked by dashed red line while the experimental data [40] are marked by dots. Inset presents the normalized specific heat as a function of the inverse reduced temperature T/T_c.

The isotropic Eliashberg equations (7)-(8) are solved iteratively until the convergence is reached, which we consider to occur when the relative variation of $\Delta(i\omega_n)$ between two consecutive iterations is lower than 10^{-9}. The number of iterations is reduced by the use of the Broyden method to predict subsequent solutions [77]. The calculations are performed for the cut-off frequency $\omega_c = 4\omega_{max}$ [78] and the number of Matsubara frequencies $M = 6500$. The self-consistent solution of Eqs. (7)-(8) for a given Eliashberg spectral function $\alpha^2F(\omega)$ is then used to calculate thermodynamic parameters and compare them with experiments.

B. Results

To determine μ^* corresponding to the experimental $T_c = 2.55$ K, we solved the equation $\Delta_{n=1}(T = 2.55\ \text{K}) = 0$ for different μ^*, see Fig. 9. The value of μ^* for which $\Delta_{n=1}(T = 2.55\ \text{K}) = 0$ defines the effective Coulomb parameter which should be taken into account to correctly evaluate thermodynamic parameters of $ThCoC_2$. As shown in Fig. 9, in the case with SOC, this procedure gives a relatively large value of $\mu^* = 0.268$, larger than 0.22 required to get the experimental value of T_c from Eliashberg formalism in $LaNiC_2$ [30]. To be compared with μ^* used with the T_c equation (5) it should be scaled to $\widetilde{\mu^*}$ according to the equation [60]

$$\frac{1}{\widetilde{\mu^*}} = \frac{1}{\mu^*} + \ln\left(\frac{\omega_c}{\omega_{\max}}\right), \tag{10}$$

which with the cut-off frequency of $\omega_c = 4\omega_{max}$ gives $\widetilde{\mu^*} = 0.195$, again larger than typically used μ^* values, similarly when the Allen-Dynes formula was applied.

The temperature dependence of $\Delta_{n=1}$ for $\mu^* = 0.268$ is presented in the inset of Fig. 9 and undergoes the following formula

$$\Delta(T) = \Delta(0)\sqrt{1 - \left(\frac{T}{T_c}\right)^{\Gamma}}, \tag{11}$$

with $\Gamma = 3.31 \pm 0.01$ slightly larger than predicted from the BCS theory, $\Gamma_{BCS} \approx 3.0$. The extrapolated $\Delta(0) = 0.39$ meV gives the dimensionless ratio $R_\Delta = 2\Delta(0)/k_BT_c = 3.55$ close to the BCS value 3.53. If not stated otherwise, in the further part of this work we present results with SOC.

For an interacting electron-phonon system, the energy difference between the superconducting and normal state ΔF is given by

$$\frac{\Delta F}{N(E_F)} = -\pi k_B T \sum_n \left(\sqrt{\omega_n^2 + \Delta_n^2} - |\omega_n|\right) \times \left(Z^S(i\omega_n) - Z^N(i\omega_n)\frac{|\omega_n|}{\sqrt{\omega_n^2 + \Delta_n^2}}\right), \tag{12}$$

where $N(E_F)$ corresponds to the density of states at the Fermi level while Z^S and Z^N denote the mass renormalization factors for the superconducting (S) and normal (N) states, respectively. Then, the difference in the electronic specific heat $\Delta C_e = C_e^S - C_e^N$ can be expressed as

$$\frac{\Delta C_e(T)}{k_B N(E_F)} = -\frac{1}{\beta}\frac{d^2\Delta F/N(E_F)}{d(k_BT)^2}, \tag{13}$$

with the specific heat in the normal state given by

$$\frac{C_e^N(T)}{k_B N(E_F)} = \frac{\pi^2}{3}k_BT(1+\lambda), \tag{14}$$

where λ is the electron-phonon coupling constant.

The temperature dependence of the specific heat is presented in Fig. 10 with the experimental data from

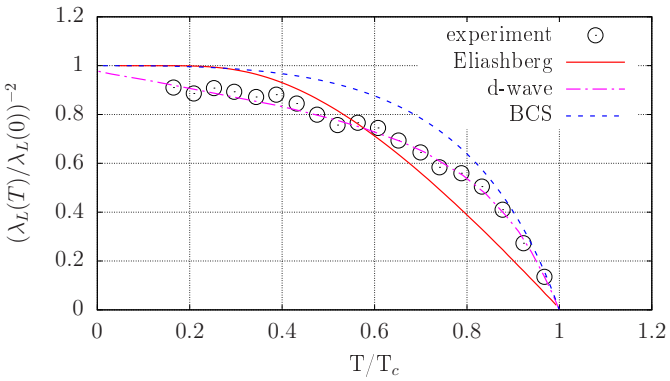


FIG. 11. Temperature dependence of the inverse normalized magnetic penetration depth λ_L^{-2}. Experimental data from the μSR measurements, marked with dots, as well as the d-wave fit are taken from Ref. 42.

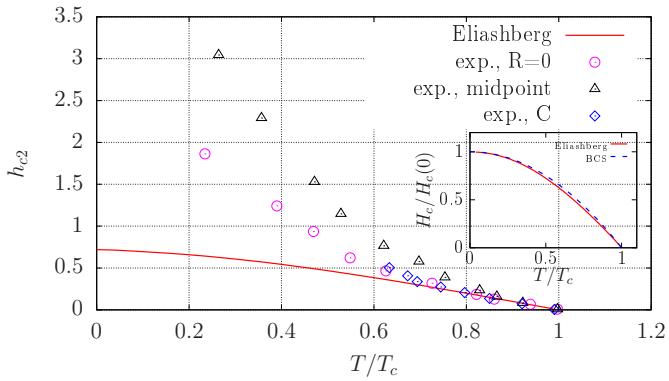


FIG. 12. Upper critical field $h_{c2} = H_{c2}(T)/T_c H'_{c2}(T_c)$ as a function of the reduced temperature T/T_c, comparison with the experiment [40]. Inset presents the comparison of the thermodynamic critical field calculated within the BCS and Eliashberg theories.

Ref. [40] plotted by dots. For comparison, BCS results are also displayed. The BCS theory of superconductivity predicts the exponential behavior of the electronic specific heat at low temperatures, in the form $C_e \propto \exp[-\Delta(0)/k_BT]$. As shown in the inset of Fig. 10, which displays the logarithmic graph of the electronic specific heat versus the inverse reduced temperature (T_c/T), the experimental curve deviates from the linear plot, expected for weakly coupled superconductors. Interestingly, at low temperatures, also the Eliashberg solution deviates from the linear BCS behavior. This demonstrates that the non-BCS behavior of C_e may occur even for the isotropic s-wave gap symmetry, if the retardation effects in the electron-phonon interactions are included as done in the Eliashberg formalism [79]. The deviation, however, is not as strong as observed experimentally [40]. At higher temperatures the Eliashberg solution approaches the BCS behavior and again deviates from the experimental data reaching the jump of reduced specific heat at T_c, $\Delta C_e/\gamma T_c = 1.425$, higher than the experimental 0.86, and almost equal to the weak-coupling BCS limit of 1.43.

Although as presented above, the deviation from a purely exponential behavior in the electronic specific heat measurement does not prejudge the nodal line superconductivity in $ThCoC_2$, recent μSR measurements [42] of the temperature dependence of the magnetic field penetration depth gave a strong support to the nodal superconductivity hypothesis, where the d-wave gap symmetry was proposed. Within the Eliashberg model, the London penetration depth λ_L can be calculated from the expression

$$\frac{1}{e^2 v_F^2 N(E_F)\lambda_L^2(T)} = \frac{2}{3}\pi k_B T \sum_n \frac{\Delta_n^2}{Z^S(i\omega_n)[\omega_n^2+\Delta_n^2]^{3/2}}, \tag{15}$$

where e is the electron charge and v_F is the Fermi velocity [78].

Figure 11 displays the comparison of the temperature dependence of the normalized penetration depth λ_L^{-2} from the μSR measurements, d-wave fit (both from [42]), our calculations [1], and the BCS theory. As in the case of the specific heat, the Eliashberg theory leads to a non-BCS curve, and the differences are more pronounced than in the case of C_e. More importantly, the isotropic Eliashberg solution significantly deviates from the experimental data in both the lower and upper T/T_c range. Much better agreement between the experimental data and theory was obtained in Ref. [42] under the assumption of the d-wave gap symmetry. Thus, temperature dependence of both the electronic specific heat and magnetic field penetration depth cannot be described by the isotropic Eliashberg formalism which supports the possibility of a non-s-wave gap symmetry in $ThCoC_2$.

A competitive concept on the nature of superconductivity in $ThCoC_2$ concerns multiband effects which are strongly indicted by the critical magnetic field measurements with the change of the $H_{c2}(T)$ curvature reported in Ref. [40]. The upper critical field within the Eliashberg model can be evaluated based on equations [78]

$$\tilde{\Delta}(i\omega_n) = \pi k_B T \sum_{n'} \frac{[\lambda(n-n') - \mu^*\theta(\omega_c - \omega_{n'})]\,\tilde{\Delta}(i\omega_{n'})}{\chi^{-1}[\tilde{\omega}(i\omega_{n'})] - \pi t^+}, \tag{16}$$

where

$$\tilde{\omega}(i\omega_n) = \omega_n + \pi k_B T \sum_{n'} \lambda(n-n')\mathrm{sgn}(\omega_{n'}) + \pi t^+ \mathrm{sgn}(\omega_{n'}), \tag{17}$$

with $t^+ = \frac{1}{2\pi\tau}$ where τ is the electronic scattering time due to the presence of impurities. In Eq. (16) the function

[1] For calculations presented in Fig. 11 to keep the consistency with the experimental results, we used $T_c = 2.3$ K as measured for the sample studied in Ref. [42]. That required taking slightly larger value of $\mu^* = 0.29$.

$\chi(\tilde{\omega})$ is given by

$$\chi(\tilde{\omega}(i\omega_n)) = \frac{2}{\sqrt{\alpha}} \int_0^\infty dq\, e^{-q^2} \tan^{-1}\left(\frac{\sqrt{\alpha}q}{|\tilde{\omega}(i\omega_n)|}\right), \quad (18)$$

with

$$\alpha(T) = \frac{1}{2}|e|H_{c2}(T)v_F^2, \quad (19)$$

where e is the elementary charge and v_F is the Fermi velocity. To evaluate τ we have calculated the electrical conductivity σ tensor for $ThCoC_2$ using the Boltzmann formalism in the constant scattering time approximation, as implemented in the BOLTZTRAP code [80]. In this approach and assuming that the electronic scattering time τ is independent of **k**-vector one may calculate the ratio of σ/τ. The computed value, averaged over directions, is $\sigma/\tau = 17.3 \times 10^{19}\ \Omega^{-1}\ \mathrm{m}^{-1}\ \mathrm{s}^{-1}$. The measured residual resistivity for the polycrystalline sample of $ThCoC_2$ is $\rho_0 = 0.37\ \mu\Omega$cm [40], which gives relatively large value of $\tau = 1.56 \times 10^{-12}$ s which originates from the high quality of the sample studied in Ref. [40] with low amount of defects. Estimated value of τ results in $t^+ = 6.71 \times 10^{-5}$ eV to be used in the above-mentioned formulas, and corresponds to the clean limit. The obtained temperature dependence of the normalized upper critical field $h_{c2} = H_{c2}(T)/T_c \frac{dH_{c2}(T_c)}{dT}$ is shown in Fig. 12 where the inset additionally presents the thermodynamic critical field $\frac{H_c}{\sqrt{N(E_F)}} = \sqrt{-8\pi \frac{\Delta F}{N(E_F)}}$ from the BCS model and Eliashberg theory. For comparison, the experimental data from different experimental methods of extraction, that is, from resistivity and specific heat measurements, are also presented.

As expected, within the one-band Eliashberg model, the curvature of h_{c2} is preserved in whole range of T/T_c indicating that the change of the curvature in the experimental curve may indeed result from multiband effects, not captured in the model presented here. Note moreover that the fully angle-resolved critical field measurements could shed light on the symmetry of the gap [81] but they are yet to be done.

C. Isotope effect

The experiment which should help to distinguish between the electron-phonon pairing mechanism in $ThCoC_2$, supported by our calculations, *versus* spin fluctuation mechanisms proposed in Ref. [42] is the measurement of the isotope effect. The isotope effect is usually described by the power law $T_c \propto M^{-\alpha}$, where M is the isotope's mass, and its presence clearly indicates the role of atomic vibrations in the superconductivity of the studied system. In our case of $ThCoC_2$, isotope effect can be measured only for carbon, which has two stable isotopes, ^{12}C with the abundance of about 98.9% and ^{13}C with 1.1% [82]. The isotope effect exponent, however, may

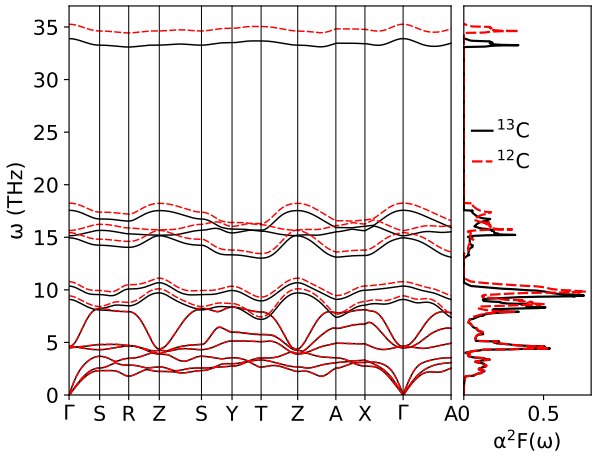


FIG. 13. Phonon dispersion relations and Eliashberg functions of $ThCoC_2$ calculated with ^{12}C and ^{13}C carbon isotopes.

differ significantly from the model $\alpha = 0.50$ value, especially in the multi-atomic compounds, depending on the details of the phonon spectrum and electron-phonon interaction. For example, in $MgCNi_3$ [83] a strong isotope effect was observed, as T_c dropped by 0.3 K when ^{12}C was fully replaced with ^{13}C, giving $\alpha = 0.54(3)$. On the other hand, in borocarbide YNi_2B_2C, significant isotope effect was observed only for boron atoms, with $\alpha \simeq 0.2$, being negligible for carbon [84, 85]. The difference in the atomic mass of the constituent elements is an important factor in determining the magnitude of the isotope effect in multiatomic compounds. This can be illustrated using the binary LiBi as an example, as it is built from the heaviest and the lightest stable solid elements. In this superconductor, the replacement of the natural Li (average mass 6.94 u) with the lighter ^{6}Li increased T_c by 0.02 K from 2.45 K to 2.47 K, resulting in an exponent $\alpha = 0.04$ [86]. Even though the effect was very weak, it was possible to determine it experimentally and theoretically [87]. Although for the present case of $ThCoC_2$ due to its deviations form the isotropic Eliashberg superconductivity we cannot provide an accurate prediction on the change in T_c, we may simulate how the phonon spectra and electron-phonon coupling is modified upon isotope substitution and estimate the variation in T_c using the conventional approach.

Phonon dispersion relations and Eliashberg functions calculated for ^{12}C and ^{13}C isotopes are shown in Fig. 13. Heavier C atoms resulted in the lowering of frequencies of the six highest optical modes of carbon, not affecting Co and Th modes. In addition, to simulate the measurements for the samples with a partial ^{12}C-^{13}C substitution, calculations were done with a C mass between 12 u and 13 u with a step of 0.2 u, not shown here for the sake of clarity. With these new Eliashberg functions, the effect of the carbon mass on T_c was simulated using both the Allen-Dynes formula and the Eliashberg formalism. Other relevant parameters were unchanged and correspond to the values which are used to reproduce

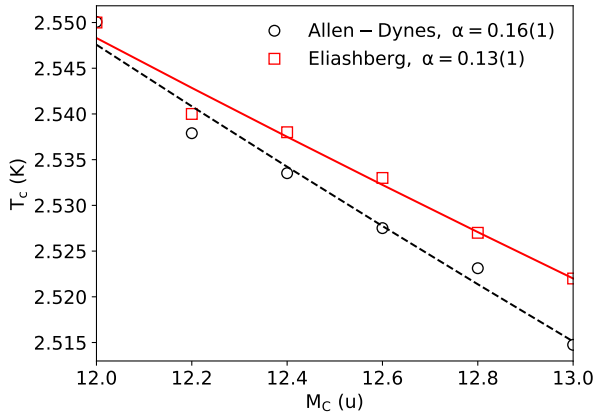


FIG. 14. Critical temperature of $ThCoC_2$ as a function of C atom's mass (open symbols) calculated using the Allen-Dynes formula or Eliashberg equations. Curves are the power law fits, $T_c = \text{const} \times M^{-\alpha}$.

the experimental $T_c = 2.55$ K for the ^{12}C case. In the Eliashberg formalism, the cutoff frequency $\omega_c = 4\omega_{\max}$ was adopted according to the shift in the frequency of the highest carbon mode. Results are presented in Fig. 14 and decrease of T_c by 0.035 K for the full ^{13}C substitution is noted. The isotope effect exponents of $\alpha = 0.13(1)$ and $\alpha = 0.16(1)$ are predicted based on the Eliashberg formalism and Allen-Dynes formula, respectively. When the Allen-Dynes formula is used, the drop in T_c is intuitively explained as resulting from the decrease in $\langle\omega_{\log}^{\alpha^2 F}\rangle$ due to ^{13}C substitution (5.816 THz to 5.717 THz) whereas λ remained almost unchanged (increase from 0.5902 to 0.5906). The predicted effect is not strong, but still larger than e.g. in LiBi, thus its experimental detection should be possible, once a set of samples with different ^{13}C content is synthesized under the same conditions.

Two comments have to be added to the discussion of the isotope effect in $ThCoC_2$. First, the predicted shift in the phonon frequencies upon ^{13}C substitution is an effect independent of superconductivity or gap symmetry. Thus, regardless of the method used to determine T_c, if the electron-phonon coupling is the pairing interaction, the magnitude of the shift in T_c should be reasonably predicted, since generally $T_c \propto \omega_c$ with ω_c being the characteristic phonon frequency. Second, the sole observation of the isotope effect does not exclude the spin fluctuations as the pairing interaction, as the interplay between electron-phonon and spin-fluctuations leads to the presence of the isotope effect in cuprates, like YBCO [88]. There, the antiferromagnetic spin fluctuations are considered as the dominant pairing interaction, which compete with the weaker electron-phonon coupling, responsible for the isotope effect. Spin fluctuations are predicted [88] to reduce the isotope effect exponent α, with the resulting magnitude depending on the relative strength of spin fluctuations and electron-phonon coupling. In the case of $ThCoC_2$, under the assumption of a dominant electron-phonon coupling and possible accompanying weak paramagnetic spin fluctuations, only a small renormalization of the isotope effect exponent from that determined by phonons can be expected [89]. Concluding, an experimental analysis of the isotope effect should deliver important results for the determination of the pairing mechanism.

VI. SUMMARY AND DISCUSSION

In summary, we have presented theoretical studies of the electronic structure, lattice dynamics, electron-phonon interaction, and superconductivity in noncentrosymmetric $ThCoC_2$. Calculations show that all atoms contribute to the Fermi surface, which in the scalar-relativistic case consists of two parts: a complex large hole-like sheet and a very small electron pocket. Spin-orbit interaction splits the electronic bands with a quite large average energy splitting of $\overline{\Delta E_{SOC}} = 150$ meV, which leads to the appearance of two dominating hole-like Fermi surface sheets. Due to the large differences in the atomic masses of the constituent atoms, in the phonon spectrum of $ThCoC_2$ we may distinguish the regions dominated by each of the atoms' vibrations: Th below 5 THz, Co between 5 and 8 THZ, and C between 8 and 35 THz. The strongest electron-phonon interaction, in the sense of the largest phonon linewidths $\gamma_{\boldsymbol{q}\nu}$ is associated with the carbon atoms' phonon modes. However, due to the lower phonon frequencies, the cobalt and thorium phonon modes also provide important contributions to the overall electron-phonon coupling parameter, calculated to be $\lambda = 0.59$. As far as the phonon properties are concerned, a negligible effect of SOC was found both for phonon dispersion relations and electron-phonon coupling function $\alpha^2F(\omega)$. Combination of the calculated density of states at the Fermi level, $N(E_F)$, and the electron-phonon coupling parameter λ lead to the theoretical value of the renormalized Sommerfeld electronic specific heat coefficient $\gamma = \gamma_{\text{band}}(1+\lambda) = 8.0$ (mJ mol^{-1} K^{-2}), slightly lower than the experimental one, $\gamma_{\text{expt}} = 8.4$ (mJ mol^{-1} K^{-2}). On the other hand, the superconducting critical temperature is overestimated, when calculated using the Allen-Dynes formula with the standard Coulomb pseudopotential parameter value (4.2 K for $\mu^* = 0.13$), and the experimental $T_c = 2.55$ K is reproduced for a relatively large value of $\mu^* = 0.165$.

That may suggest the presence of other depairing mechanisms like electron-paramagnon interactions, which effectively enhance μ^*. However, in connection with the unusual thermodynamic properties, it rather indicates that the superconductivity is not isotropic s-wave-like, and due to the strong spin-orbit coupling the Allen-Dynes formula may overestimate T_c.

Additionally, the thermodynamic properties of the superconducting phase in $ThCoC_2$ were analyzed with the help of the isotropic Eliashberg equations. A non-BCS temperature dependence of the electronic specific heat and the London penetration depth were found. In con-

trary to the sister compound, $LaNiC_2$, for which the Allen-Dynes formula worked well and temperature dependence of the London penetration depth was close to that predicted by the isotropic Eliashberg formalism [30], in the case of $ThCoC_2$ the experimental results are far from those predicted by the isotropic theory. Similarly, the measured temperature dependence of the upper magnetic critical field is not explained in terms of the s-wave single-band model. Those features are likely to be driven by the strong SOC found in $ThCoC_2$, as in the limit of the strong spin-orbit interaction [2], the pairing inside the spin-split bands requires the odd parity of the gap with respect to the $\mathbf{k} \to -\mathbf{k}$. This opens the possibility of a non-s-like gap symmetry in $ThCoC_2$, which is achievable even with the electron-phonon-based pairing [90–92].

Concluding, in view of our results, the electron-phonon interaction is strong enough to mediate the superconductivity in $ThCoC_2$, but the measured thermodynamic properties of the superconducting phase much deviate from those predicted by the isotropic Eliashberg theory. Further works are thus required to distinguish between the phonon and spin-fluctuation mechanisms, proposed along with the d-wave gap symmetry in Ref. [42]. Our calculations show that the analysis of the carbon isotope effect could yield important results. In spite of the large mass differences between Th, Co and C, observation of the isotope effect on C is predicted, with an exponent $\alpha \simeq 0.15$.

ACKNOWLEDGEMENTS

This work was supported by the National Science Centre (Poland), project No. 2017/26/E/ST3/00119 and in part by the PL-Grid Infrastructure (allocation of computing time).

[1] Lev P. Gor'kov and Emmanuel I. Rashba, "Superconducting 2D System with Lifted Spin Degeneracy: Mixed Singlet-Triplet State," Phys. Rev. Lett. **87**, 037004 (2001).

[2] K. V. Samokhin, E. S. Zijlstra, and S. K. Bose, "$CePt_3Si$: An unconventional superconductor without inversion center," Phys. Rev. B **69**, 094514 (2004).

[3] P. A. Frigeri, D. F. Agterberg, A. Koga, and M. Sigrist, "Superconductivity without Inversion Symmetry: MnSi versus $CePt_3Si$," Phys. Rev. Lett. **92**, 097001 (2004).

[4] Satoshi Fujimoto, "Electron Correlation and Pairing States in Superconductors without Inversion Symmetry," Journal of the Physical Society of Japan **76**, 051008 (2007), https://doi.org/10.1143/JPSJ.76.051008.

[5] S. K. Yip, "Two-dimensional superconductivity with strong spin-orbit interaction," Phys. Rev. B **65**, 144508 (2002).

[6] E. Bauer, G. Hilscher, H. Michor, Ch. Paul, E. W. Scheidt, A. Gribanov, Yu. Seropegin, H. Noël, M. Sigrist, and P. Rogl, "Heavy Fermion Superconductivity and Magnetic Order in Noncentrosymmetric $CePt_3Si$," Phys. Rev. Lett. **92**, 027003 (2004).

[7] N. Kimura, K. Ito, H. Aoki, S. Uji, and T. Terashima, "Extremely High Upper Critical Magnetic Field of the Noncentrosymmetric Heavy Fermion Superconductor $CeRhSi_3$," Phys. Rev. Lett. **98**, 197001 (2007).

[8] Rikio Settai, Yuichiro Miyauchi, Tetsuya Takeuchi, Florence Lévy, Ilya Sheikin, and Yoshichika Ōnuki, "Huge Upper Critical Field and Electronic Instability in Pressure-induced Superconductor $CeIrSi_3$ without Inversion Symmetry in the Crystal Structure," Journal of the Physical Society of Japan **77**, 073705 (2008), https://doi.org/10.1143/JPSJ.77.073705.

[9] K. Togano, P. Badica, Y. Nakamori, S. Orimo, H. Takeya, and K. Hirata, "Superconductivity in the Metal Rich Li-Pd-B Ternary Boride," Phys. Rev. Lett. **93**, 247004 (2004).

[10] Petre Badica, Takaaki Kondo, and Kazumasa Togano, "Superconductivity in a New Pseudo-Binary $Li_2B(Pd_{1-x}Pt_x)_3$ ($x = 0 - 1$) Boride System," Journal of the Physical Society of Japan **74**, 1014–1019 (2005), https://doi.org/10.1143/JPSJ.74.1014.

[11] M. Nishiyama, Y. Inada, and Guo-qing Zheng, "Spin Triplet Superconducting State due to Broken Inversion Symmetry in Li_2Pt_3B," Phys. Rev. Lett. **98**, 047002 (2007).

[12] H. Q. Yuan, D. F. Agterberg, N. Hayashi, P. Badica, D. Vandervelde, K. Togano, M. Sigrist, and M. B. Salamon, "S-Wave Spin-Triplet Order in Superconductors without Inversion Symmetry: Li_2Pd_3B and Li_2Pt_3B," Phys. Rev. Lett. **97**, 017006 (2006).

[13] K.-W. Lee and W. E. Pickett, "Crystal symmetry, electron-phonon coupling, and superconducting tendencies in Li_2Pd_3B and Li_2Pt_3B," Phys. Rev. B **72**, 174505 (2005).

[14] T. Klimczuk, F. Ronning, V. Sidorov, R. J. Cava, and J. D. Thompson, "Physical Properties of the Noncentrosymmetric Superconductor $Mg_{10}Ir_{19}B_{16}$," Phys. Rev. Lett. **99**, 257004 (2007).

[15] Yanpeng Qi, Jiangang Guo, Hechang Lei, Zewen Xiao, Toshio Kamiya, and Hideo Hosono, "Superconductivity in noncentrosymmetric ternary equiatomic pnictides LaMP (M = Ir and Rh; P = P and As)," Phys. Rev. B **89**, 024517 (2014).

[16] Lei Fang, Huan Yang, Xiyu Zhu, Gang Mu, Zhao-Sheng Wang, Lei Shan, Cong Ren, and Hai-Hu Wen, "Physical properties of the noncentrosymmetric superconductor Ru_7B_3," Phys. Rev. B **79**, 144509 (2009).

[17] Naoki Kase and Jun Akimitsu, "Superconducting State of the Binary Boride Ru_7B_3 with the Noncentrosymmetric Crystal Structure," Journal of the Physical Society of Japan **78**, 044710 (2009), https://doi.org/10.1143/JPSJ.78.044710.

[18] J. Chen, M. B. Salamon, S. Akutagawa, J. Akimitsu, J. Singleton, J. L. Zhang, L. Jiao, and H. Q. Yuan, "Evidence of nodal gap structure in the noncentrosymmetric superconductor Y_2C_3," Phys. Rev. B **83**, 144529 (2011).

[19] S. Kuroiwa, Y. Saura, J. Akimitsu, M. Hiraishi, M. Miyazaki, K. H. Satoh, S. Takeshita, and R. Kadono, "Multigap Superconductivity in Sesquicarbides La_2C_3 and Y_2C_3," Phys. Rev. Lett. **100**, 097002 (2008).

[20] E. Bauer, G. Rogl, Xing-Qiu Chen, R. T. Khan, H. Michor, G. Hilscher, E. Royanian, K. Kumagai, D. Z. Li, Y. Y. Li, R. Podloucky, and P. Rogl, "Unconventional superconducting phase in the weakly correlated noncentrosymmetric Mo_3Al_2C compound," Phys. Rev. B **82**, 064511 (2010).

[21] Elizabeth M. Carnicom, Weiwei Xie, Tomasz Klimczuk, Jingjing Lin, Karolina Górnicka, Zuzanna Sobczak, Nai Phuan Ong, and Robert J. Cava, "$TaRh_2B_2$ and $NbRh_2B_2$: Superconductors with a chiral noncentrosymmetric crystal structure," Science Advances **4** (2018), 10.1126/sciadv.aar7969.

[22] Karolina Górnicka, Xin Gui, Bartlomiej Wiendlocha, Loi T. Nguyen, Weiwei Xie, Robert J. Cava, and Tomasz Klimczuk, "NbIr2B2 and TaIr2B2 – New Low Symmetry Noncentrosymmetric Superconductors with Strong Spin–Orbit Coupling," Advanced Functional Materials **31**, 2007960 (2021).

[23] W.H. Lee, H.K. Zeng, Y.D. Yao, and Y.Y. Chen, "Superconductivity in the ni based ternary carbide $lanic_2$," Physica C: Superconductivity **266**, 138 – 142 (1996).

[24] V. K. Pecharsky, L. L. Miller, and K. A. Gschneidner, "Low-temperature behavior of two ternary lanthanide nickel carbides: Superconducting $LaNiC_2$ and magnetic $CeNiC_2$," Phys. Rev. B **58**, 497–502 (1998).

[25] Y. Iwamoto, Y. Iwasaki, K. Ueda, and T. Kohara, "Microscopic measurements in 139la-nqr of the ternary carbide superconductor $lanic_2$," Physics Letters A **250**, 439 – 442 (1998).

[26] Jorge Quintanilla, Adrian D. Hillier, James F. Annett, and R. Cywinski, "Relativistic analysis of the pairing symmetry of the noncentrosymmetric superconductor $LaNiC_2$," Phys. Rev. B **82**, 174511 (2010).

[27] I Bonalde, R L Ribeiro, K J Syu, H H Sung, and W H Lee, "Nodal gap structure in the noncentrosymmetric superconductor $LaNiC_2$from magnetic-penetration-depth measurements," New Journal of Physics **13**, 123022 (2011).

[28] J Chen, L. Jiao, J. L. Zhang, Y. Chen, L Yang, M. Nicklas, F. Steglich, and H. Q. Yuan, "Evidence for two-gap superconductivity in the non-centrosymmetric compound $LaNiC_2$," New Journal of Physics **15**, 053005 (2013).

[29] Susumu Katano, Hideya Nakagawa, Kazuyuki Matsubayashi, Yoshiya Uwatoko, Hideto Soeda, Takahiro Tomita, and Hiroki Takahashi, "Anomalous pressure dependence of the superconductivity in noncentrosymmetric $LaNiC_2$: Evidence of strong electronic correlations," Phys. Rev. B **90**, 220508(R) (2014).

[30] B. Wiendlocha, R. Szczęśniak, A. P. Durajski, and M. Muras, "Pressure effects on the unconventional superconductivity of noncentrosymmetric $LaNiC_2$," Phys. Rev. B **94**, 134517 (2016).

[31] J. F. Landaeta, D. Subero, P. Machado, F. Honda, and I. Bonalde, "Unconventional superconductivity and an ambient-pressure magnetic quantum critical point in single-crystal $LaNiC_2$," Phys. Rev. B **96**, 174515 (2017).

[32] Gábor Csire, Balázs Újfalussy, and James F Annett, "Nonunitary triplet pairing in the noncentrosymmetric superconductor $LaNiC_2$," The European Physical Journal B **91**, 1–7 (2018).

[33] Anton Kokalj, "Computer graphics and graphical user interfaces as tools in simulations of matter at the atomic scale," Computational Materials Science **28**, 155 – 168 (2003).

[34] Shyam Sundar, S. R. Dunsiger, S. Gheidi, K. S. Akella, A. M. Côté, H. U. Özdemir, N. R. Lee-Hone, D. M. Broun, E. Mun, F. Honda, Y. J. Sato, T. Koizumi, R. Settai, Y. Hirose, I. Bonalde, and J. E. Sonier, "Two-gap time reversal symmetry breaking superconductivity in noncentrosymmetric $LaNiC_2$," Phys. Rev. B **103**, 014511 (2021).

[35] Kamil K. Kolincio, Marta Roman, Michał J. Winiarski, Judyta Strychalska-Nowak, and Tomasz Klimczuk, "Magnetism and charge density waves in $R$$NiC_2$ (R=Ce,Pr,Nd," Phys. Rev. B **95**, 235156 (2017).

[36] Marta Roman, Judyta Strychalska-Nowak, Tomasz Klimczuk, and Kamil K. Kolincio, "Extended phase diagram of $R$$NiC_2$ family: Linear scaling of the Peierls temperature," Phys. Rev. B **97**, 041103(R) (2018).

[37] S. Steiner, H. Michor, O. Sologub, B. Hinterleitner, F. Höfenstock, M. Waas, E. Bauer, B. Stöger, V. Babizhetskyy, V. Levytskyy, and B. Kotur, "Single-crystal study of the charge density wave metal $LuNiC_2$," Phys. Rev. B **97**, 205115 (2018).

[38] Marta Roman, Tomasz Klimczuk, and Kamil K. Kolincio, "Correlation between charge density waves and antiferromagnetism in $Nd_{1-x}Gd_xNiC_2$ solid solutions," Phys. Rev. B **98**, 035136 (2018).

[39] Kamil K. Kolincio, Marta Roman, and Tomasz Klimczuk, "Charge density wave and large nonsaturating magnetoresistance in $YNiC_2$ and $LuNiC_2$," Phys. Rev. B **99**, 205127 (2019).

[40] T Grant, A J S Machado, D J Kim, and Z Fisk, "Superconductivity in non-centrosymmetric $ThCoC_2$," Superconductor Science and Technology **27**, 035004 (2014).

[41] T. W. Grant, O. V. Cigarroa, P. F. S. Rosa, A. J. S. Machado, and Z. Fisk, "Tuning of superconductivity by Ni substitution into noncentrosymmetric $ThCo_{1-x}Ni_xC_2$," Phys. Rev. B **96**, 014507 (2017).

[42] A. Bhattacharyya, D. T. Adroja, K. Panda, Surabhi Saha, Tanmoy Das, A. J. S. Machado, O. V. Cigarroa, T. W. Grant, Z. Fisk, A. D. Hillier, and P. Manfrinetti, "Evidence of a Nodal Line in the Superconducting Gap Symmetry of Noncentrosymmetric $ThCoC_2$," Phys. Rev. Lett. **122**, 147001 (2019).

[43] Y. Takano, H. Takeya, H. Fujii, H. Kumakura, T. Hatano, K. Togano, H. Kito, and H. Ihara, "Superconducting properties of MgB_2 bulk materials prepared by high-pressure sintering," Applied Physics Letters **78**, 2914–2916 (2001), https://doi.org/10.1063/1.1371239.

[44] S. V. Shulga, S.-L. Drechsler, G. Fuchs, K.-H. Müller, K. Winzer, M. Heinecke, and K. Krug, "Upper Critical Field Peculiarities of Superconducting YNi_2B_2C and $LuNi_2B_2C$," Phys. Rev. Lett. **80**, 1730–1733 (1998).

[45] Paolo Giannozzi, Stefano Baroni, Nicola Bonini, Matteo Calandra, Roberto Car, Carlo Cavazzoni, Davide Ceresoli, Guido L Chiarotti, Matteo Cococcioni, Ismaila Dabo, Andrea Dal Corso, Stefano de Gironcoli, Stefano Fabris, Guido Fratesi, Ralph Gebauer, Uwe Gerstmann, Christos Gougoussis, Anton Kokalj, Michele Lazzeri, Layla Martin-Samos, Nicola Marzari, Francesco Mauri, Riccardo Mazzarello, Stefano Paolini, Alfredo

Pasquarello, Lorenzo Paulatto, Carlo Sbraccia, Sandro Scandolo, Gabriele Sclauzero, Ari P Seitsonen, Alexander Smogunov, Paolo Umari, and Renata M Wentzcovitch, "QUANTUM ESPRESSO: a modular and open-source software project for quantum simulations of materials," Journal of Physics: Condensed Matter **21**, 395502 (2009).

[46] P Giannozzi, O Andreussi, T Brumme, O Bunau, M Buongiorno Nardelli, M Calandra, R Car, C Cavazzoni, D Ceresoli, M Cococcioni, N Colonna, I Carnimeo, A Dal Corso, S de Gironcoli, P Delugas, R A DiStasio Jr, A Ferretti, A Floris, G Fratesi, G Fugallo, R Gebauer, U Gerstmann, F Giustino, T Gorni, J Jia, M Kawamura, H-Y Ko, A Kokalj, E Kucukbenli, M Lazzeri, M Marsili, N Marzari, F Mauri, N L Nguyen, H-V Nguyen, A Otero de-la Roza, L Paulatto, S Ponce, D Rocca, R Sabatini, B Santra, M Schlipf, A P Seitsonen, A Smogunov, I Timrov, T Thonhauser, P Umari, N Vast, X Wu, and S Baroni, "Advanced capabilities for materials modelling with QUANTUM ESPRESSO," Journal of Physics: Condensed Matter **29**, 465901 (2017).

[47] John P. Perdew, Kieron Burke, and Matthias Ernzerhof, "Generalized Gradient Approximation Made Simple," Phys. Rev. Lett. **77**, 3865–3868 (1996).

[48] Pseudopotential were accessed from https://www.quantum-espresso.org/pseudopotentials. The following files were used: Th.pbe-spfn-rrkjus_psl.1.0.0.UPF, Th.rel-pbe-spfn-rrkjus_psl.1.0.0.UPF, Co.pbe-spn-rrkjus_psl.0.3.1.UPF, Co.rel-pbe-spn-rrkjus_psl.0.3.1.UPF and C.pbe-n-rrkjus_psl.1.0.0.UPF.

[49] Andrea Dal Corso, "Pseudopotentials periodic table: From H to Pu," Computational Materials Science **95**, 337 – 350 (2014).

[50] M.H. Gerss and W. Jeitschko, "The crystal structures of ternary actinoid iron (cobalt, nickel) carbides with composition 1:1:2," Materials Research Bulletin **21**, 209 – 216 (1986).

[51] Stefano Baroni, Stefano de Gironcoli, Andrea Dal Corso, and Paolo Giannozzi, "Phonons and related crystal properties from density-functional perturbation theory," Rev. Mod. Phys. **73**, 515–562 (2001).

[52] M Smidman, M B Salamon, H Q Yuan, and D F Agterberg, "Superconductivity and spin-orbit coupling in non-centrosymmetric materials: a review," Reports on Progress in Physics **80**, 036501 (2017).

[53] L. Jiao, J. L. Zhang, Y. Chen, Z. F. Weng, Y. M. Shao, J. Y. Feng, X. Lu, B. Joshi, A. Thamizhavel, S. Ramakrishnan, and H. Q. Yuan, "Anisotropic superconductivity in noncentrosymmetric BiPd," Phys. Rev. B **89**, 060507(R) (2014).

[54] Mitsuaki Kawamura, "Fermisurfer: Fermi-surface viewer providing multiple representation schemes," Computer Physics Communications **239**, 197 – 203 (2019).

[55] Kevin T. Moore and Gerrit van der Laan, "Nature of the $5f$ states in actinide metals," Rev. Mod. Phys. **81**, 235–298 (2009).

[56] Karolina Górnicka, Debarchan Das, Sylwia Gutowska, Bartłomiej Wiendlocha, Michał J. Winiarski, Tomasz Klimczuk, and Dariusz Kaczorowski, "Iridium $5d$-electron driven superconductivity in $ThIr_3$," Phys. Rev. B **100**, 214514 (2019).

[57] R. Heid, K.-P. Bohnen, I. Yu. Sklyadneva, and E. V. Chulkov, "Effect of spin-orbit coupling on the electron-phonon interaction of the superconductors Pb and Tl," Phys. Rev. B **81**, 174527 (2010).

[58] Sylwia Gołab and Bartlomiej Wiendlocha, "Electron-phonon superconductivity in $CaBi_2$ and the role of spin-orbit interaction," Phys. Rev. B **99**, 104520 (2019).

[59] H. M. Tütüncü, Ertuğrul Karaca, H. Y. Uzunok, and G. P. Srivastava, "Role of spin-orbit coupling in the physical properties of LaX_3 (X = In, P, Bi) superconductors," Phys. Rev. B **97**, 174512 (2018).

[60] P. B. Allen and R. C. Dynes, "Transition temperature of strong-coupled superconductors reanalyzed," Phys. Rev. B **12**, 905–922 (1975).

[61] N. F. Berk and J. R. Schrieffer, "Effect of Ferromagnetic Spin Correlations on Superconductivity," Phys. Rev. Lett. **17**, 433–435 (1966).

[62] H. Rietschel and H. Winter, "Role of Spin Fluctuations in the Superconductors Nb and V," Phys. Rev. Lett. **43**, 1256–1260 (1979).

[63] J. M. Daams, B. Mitrović, and J. P. Carbotte, "Simulation of the Effects of Paramagnons on a Superconductor by a Simple Rescaling," Phys. Rev. Lett. **46**, 65–68 (1981).

[64] O. V. Dolgov, I. I. Mazin, A. A. Golubov, S. Y. Savrasov, and E. G. Maksimov, "Critical Temperature and Enhanced Isotope Effect in the Presence of Paramagnons in Phonon-Mediated Superconductors," Phys. Rev. Lett. **95**, 257003 (2005).

[65] C. Candolfi, B. Lenoir, A. Dauscher, C. Bellouard, J. Hejtmánek, E. Šantavá, and J. Tobola, "Spin Fluctuations and Superconductivity in Mo_3Sb_7," Phys. Rev. Lett. **99**, 037006 (2007).

[66] B. Wiendlocha, J. Tobola, M. Sternik, S. Kaprzyk, K. Parlinski, and A. M. Oleś, "Superconductivity of Mo_3Sb_7 from first principles," Phys. Rev. B **78**, 060507 (2008).

[67] S. Y. Savrasov and D. Y. Savrasov, "Electron-phonon interactions and related physical properties of metals from linear-response theory," Phys. Rev. B **54**, 16487–16501 (1996).

[68] K. Jasiewicz, B. Wiendlocha, K. Górnicka, K. Gofryk, M. Gazda, T. Klimczuk, and J. Tobola, "Pressure effects on the electronic structure and superconductivity of $(TaNb)_{0.67}(HfZrTi)_{0.33}$ high entropy alloy," Phys. Rev. B **100**, 184503 (2019).

[69] Alaska Subedi and David J. Singh, "Electron-phonon superconductivity in noncentrosymmetric $LaNiC_2$: First-principles calculations," Phys. Rev. B **80**, 092506 (2009).

[70] G. M. Eliashberg, "Interactions between electrons and lattice vibrations in a superconductor," Soviet Physics-JETP **11**, 696 (1960).

[71] P Morel and P W Anderson, "Calculation of the superconducting state parameters with retarded electron-phonon interaction," Phys. Rev. **125**, 1263 (1962).

[72] Warren E. Pickett, "Generalization of the theory of the electron-phonon interaction: Thermodynamic formulation of superconducting- and normal-state properties," Phys. Rev. B **26**, 1186–1207 (1982).

[73] Chang-Youn Moon, Yong-Hyun Kim, and K. J. Chang, "Dielectric-screening properties and Coulomb pseudopotential μ^* for MgB_2," Phys. Rev. B **70**, 104522 (2004).

[74] Antonio Sanna, José A. Flores-Livas, Arkadiy Davydov, Gianni Profeta, Kay Dewhurst, Sangeeta Sharma, and E. K. U. Gross, "Ab initio Eliashberg Theory: Making Genuine Predictions of Superconducting Features," Journal of the Physical Society of Japan **87**, 041012 (2018).

[75] R. Szczęśniak, A.P. Durajski, and Ł. Herok, "Thermodynamic properties of antiperovskite $MgCNi_3$ in superconducting phase," Solid State Communications **203**, 63 – 68 (2015).

[76] Sylwia Gutowska, Karolina Górnicka, Paweł Wójcik, Tomasz Klimczuk, and Bartlomiej Wiendlocha, "Strong-coupling superconductivity of $srir_2$ and $srrh_2$: Phonon engineering of metallic ir and rh," Phys. Rev. B **104**, 054505 (2021).

[77] G P Srivastava, "Broyden's method for self-consistent field convergence acceleration," J. Phys. A: Math. Gen. **17**, 2737 (1984).

[78] J. P. Carbotte, "Properties of boson-exchange superconductors," Rev. Mod. Phys. **62**, 1027–1157 (1990).

[79] A. P. Durajski, R. Szczęśniak, and Y. Li, "Non-bcs thermodynamic properties of h_2s superconductor," Physica C: Superconductivity and its Applications **515**, 1 – 6 (2015).

[80] Georg K.H. Madsen and David J. Singh, "BoltzTraP. A code for calculating band-structure dependent quantities," Computer Physics Communications **175**, 67–71 (2006).

[81] Jing-Rong Wang, Guo-Zhu Liu, and Chang-Jin Zhang, "Connection between in-plane upper critical field H_{c2} and gap symmetry in layered d-wave superconductors," Phys. Rev. B **94**, 014501 (2016).

[82] Alfred O. Nier, "A Redetermination of the Relative Abundances of the Isotopes of Carbon, Nitrogen, Oxygen, Argon, and Potassium," Phys. Rev. **77**, 789–793 (1950).

[83] T. Klimczuk and R. J. Cava, "Carbon isotope effect in superconducting $MgCNi_3$," Phys. Rev. B **70**, 212514 (2004).

[84] D.D. Lawrie and J.P. Franck, "Boron isotope effect in Ni and Pd based borocarbide superconductors," Physica C: Superconductivity **245**, 159 – 163 (1995).

[85] K.O. Cheon, I.R. Fisher, and P.C. Canfield, "Boron isotope effect in single-crystal YNi_2B_2C and $LuNi_2B_2C$ superconductors," Physica C: Superconductivity **312**, 35 – 39 (1999).

[86] Takashi Sambongi, "Superconductivity of LiBi," Journal of the Physical Society of Japan **30**, 294–294 (1971).

[87] Karolina Górnicka, Sylwia Gutowska, Michał J. Winiarski, Bartlomiej Wiendlocha, Weiwei Xie, R. J. Cava, and Tomasz Klimczuk, "Superconductivity on a Bi Square Net in LiBi," Chemistry of Materials **32**, 3150–3159 (2020).

[88] T. S. Nunner, J. Schmalian, and K. H. Bennemann, "Influence of electron-phonon interaction on spin-fluctuation-induced superconductivity," Phys. Rev. B **59**, 8859–8868 (1999).

[89] Hiroshi Shimahara, "Isotope effect in superconductors with coexisting interactions of phonon and nonphonon mechanisms," Journal of the Physical Society of Japan **72**, 1851–1854 (2003), https://doi.org/10.1143/JPSJ.72.1851.

[90] Karol I. Wysokinski, "Eliashberg-type equations for correlated superconductors," Phys. Rev. B **54**, 3553–3561 (1996).

[91] Karol I. Wysokiński, "Symmetry of the order parameter in correlated electron - phonon superconductor," Physica C: Superconductivity **282-287**, 1701–1702 (1997).

[92] J. P. Hague, "d-wave superconductivity from electron-phonon interactions," Phys. Rev. B **73**, 060503 (2006).